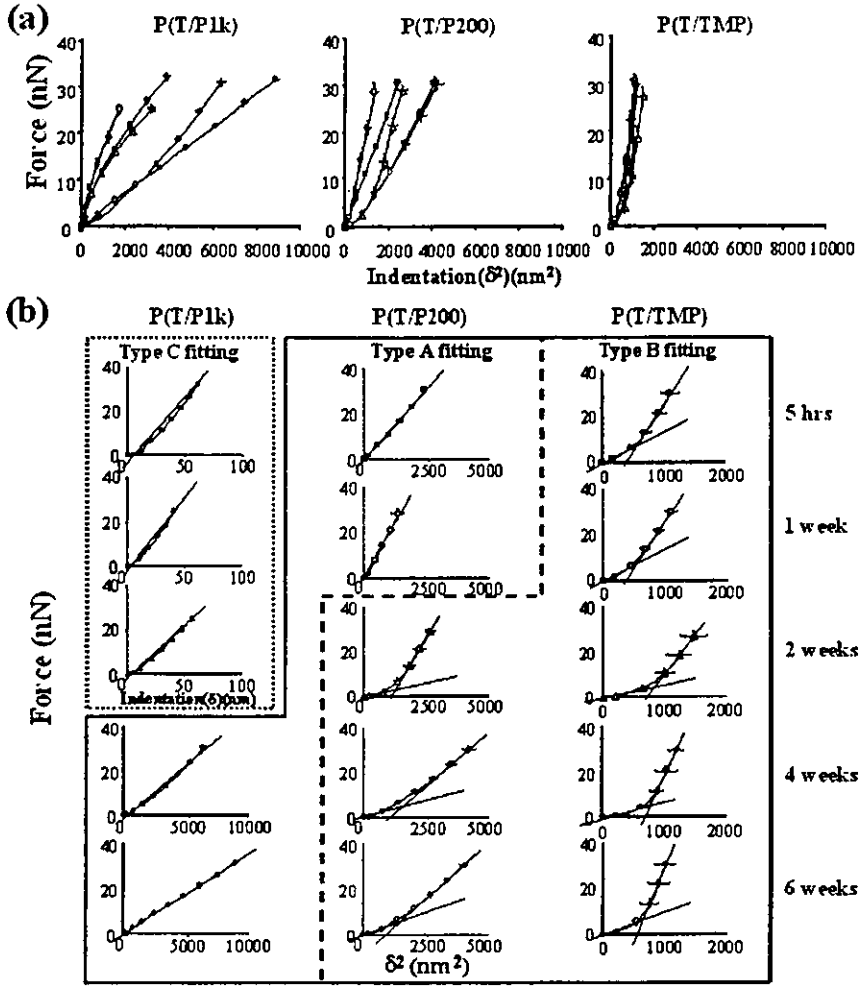

Figure 8. $F-\delta^2$ plots (a) for the analysis with Hertz model for 5 h (■), 1 week (□), 2 weeks (△), 4 weeks (●), and 6 weeks (○) of immersion in PBS and (b) three types of fitting analyses with Hertz model: linear fitting for linear $F-\delta^2$ plots using conical tip assumption (type A fitting), a biphasic fitting for biphasic $F-\delta^2$ plots using conical tip assumption (type B fitting), and linear fitting for $F-\delta$ plots using the model of a flat-ended cylindrical tip (type C fitting) (n = 7).

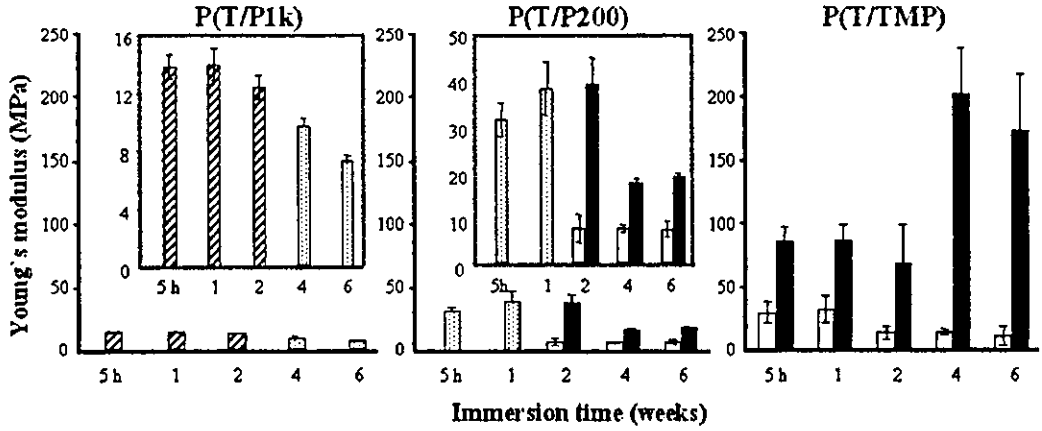

Figure 9. Young's moduli of P(T/P1k), P(T/P200), and P(T/TMP) films upon hydrolysis (n = 7).

In this study, we focused on the preparation of various types of liquid acrylated TMC-based prepolymers using triol (TMP) and linear PEGs with molecular weights of 200, 600, or 1000. The former prepolymer is trifunctional acrylated prepolymer, whereas the latter prepolymers are bifunctional acrylated prepolymers. The resultant acrylated prepolymers have molecular weights of between 800 and 2600. In the case of trifunctional prepolymer, T/TMP, the molecular weight, as obtained from standard GPC calibrated with well-defined linear PEGs, could be lower than its true molecular weight because the hydrodynamic volume of a branched molecule is smaller than that of a linear one.[22] Depending on the type of initiator and its molecular weight, comonomer, and polymer composition, the physical state of the (co)-oligomers was liquid, viscous liquid, or paste (Table 1). Upon acrylation at terminal ends of liquid (co)oligomers, acrylated

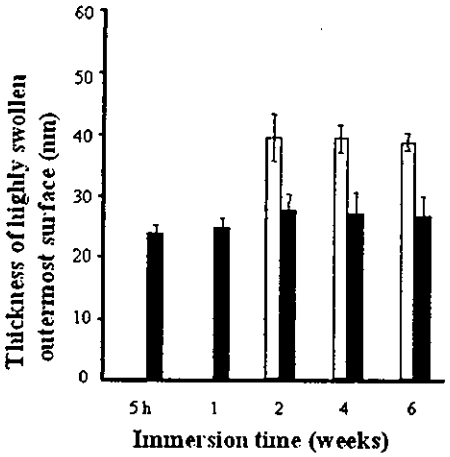

Figure 10. Thickness of the highly swollen outermost surface (T) calculated at the intersection of two-step fitting lines of the biphasic $F-\delta^2$ plot ($n = 7$).

prepolymers exhibited a rapid liquid-to-solid transformation induced by visible-light irradiation, irrespective of the type of prepolymers studied here. All of the acrylated prepolymers photocured within 10−20 s of photoirradiation at the photointensity (100 mW/cm^2) used (Figure 2). The photocuring yield increased with increasing irradiation time, photointensity (Figure 2-1), and camphorquinone concentration (Figure 2-2) but tended to decrease with increasing liquid film thickness (Figure 2-3) and molecular weight of prepolymer (Figure 2-4). These photocuring characteristics were similar to those of polymers composed of TMC and CL, which were reported in our previous paper.[19]

The wettability and time-dependent characteristics of water uptake and weight loss during hydrolysis depended on the type of photocured polymer (Figure 3). As expected, the higher degrees of water uptake and weight loss were found for **P(T/L/P1k)**, followed by **P(T/P1k)**, compared with **P(T/P200)** and **P(T/TMP)**, indicating that the hydrophilic component as an initiator, PEG1000, and faster degradable polyester, PLL, than polycarbonate are responsible for this behavior. The PEG200-based polymer, **P(T/P200)**, exhibited moderate degrees of this behavior. The lowest degrees of this behavior were observed for TMP-based **P(T/TMP)**, which lacks a hydrophilic component in the molecule and heavier cross-linking density due to trifunctional prepolymer compared with bifunctional PEG-based prepolymers (Figure 3). Topological SEM and AFM images of hydrolyzed surfaces of photocured films and swelling depth profiles of cross-sectional views of rose bengal-stained samples by CLSM clearly differentiated the hydrolytic degradation behavior of these photocured polymers. The results are summarized as follows. (1) For **P(T/P1k)**, a highly swollen rough layer was formed at an early period of immersion in water, but it became smoother upon further immersion. However, at a prolonged period, pits were created, probably due to the inhomogeneous surface composition (Figure 5). (2) The swelling and subsequent hydrolysis occurred only at the surface region of the photocured polymers **P(T/P200)** and **P(T/TMP)**, whereas **P(T/P1k)** exhibited complete swelling of the sample (Figure 6).

It is of great interest to determine how micromechanical properties of surface regions of photocured polymers are changed upon hydrolysis and their dependences on the type of photocured polymers. The force−indentation curves determined by nanoindentation using AFM differentiated the nature of water-swellable surface regions and concomitantly the microelastic modulus of the surface regions. Qualitatively, there were marked differences between the hydrolysis-time-dependent force−indentation curves of hydrolyzed samples (Figure 7). Regardless of the hydrolysis time, indentation was enhanced in the order **P(T/P1k)** > **P(T/P200)** ≫ **P(T/TMP)**. **P(T/P1k)** became significantly softer with a hydrolysis time increase. This tendency was also observed for both **P(T/P200)** and **P(T/TMP)**. However, the tendency was reduced in the order **P(T/P1k)** > **P(T/P200)** ≫ **P(T/TMP)**.

For quantitative discussion, the Hertz model was employed to determine the microelastic modulus. The linear $F-\delta^2$ relation, from which Young's modulus is determined, was obtained when a cone-type tip was used for measurement (type A fitting in Scheme 2). This was observed for **P(T/P200)** during the early period of hydrolysis. However, a concave $F-\delta^2$ relation was observed during the later period of hydrolysis. This strongly implies that surface regions are inhomogeneous in the vertical direction of surface (depth). The concave curve is divided approximately into two linear fittings. This means that a two-layer surface model (Figure 8b) approximately fits the $F-\delta^2$ curves. This allows the differentiation of the microelastic modulus of surface regions. Young's moduli at the outermost surface regions were much smaller than those at deeper regions. The approximate thickness of the highly swollen layer, which was calculated from the intersection points of two linear lines, was estimated to be approximately 40 nm, which did not change over an observation period for up to 6 weeks. This also occurred in **P(T/TMP)**, which swelled only at the outermost surface region: the thickness of the surface region with low elastic modulus was estimated to be 25−30 nm, which did not change considerably even with longer term hydrolysis (Figure 10). Taken together, these factors indicate that, for both **P(T/TMP)** and **P(T/P200)**, degradation proceeds via a surface erosion. The increased E_2 (Young's modulus of the deeper or less swellable layer) of **P(T/TMP)** observed at after a longer period of hydrolysis, as shown in Figure 9, may be due to the effect of oxygen during photopolymerization. Oxygen, diffused into the surface regions, retards or inhibits radical polymerization, resulting in a lower cross-linking density at the outer surface region than at the deeper surface region or in the bulk phase. On the other hand, as for **P(T/P1k)**, type C fitting was employed for an early period of hydrolysis, whereas type A fitting was for a later period. At this moment, we do not have any reasonable interpretation for a type C fitting (that is a linear $F-\delta$ relation) during an early period despite use of a cone-type tip in the AFM measurement. (Note that theoretically the type C fitting is observed using the flat-ended cylindrical-type AFM tip.) Regardless of the type of curve fitting, Young's moduli tended to decrease as the hydrolysis period lengthened. The estimated Young's moduli were as follows: for the highly swellable surface of **P(T/P1k)**, E ($E_1 = E_2$) was almost 10 MPa; for the less swellable surface of **P(T/P200)**, E_1 was approximately 10 MPa and E_2 ranged from 40 MPa (initial

period) to 20 MPa (later period); for the least swellable P(T/TMP), E_1 was 35 MPa (initial) to 15 MPa (later), and E_2 was approximately 100 MPa (initial) to 200 MPa (later).

The combination of a biodegradable liquid prepolymer with a photocured polymer having a wide scope of hydrolytic characteristics including surface erosion or whole-body degradation may provide a unique opportunity for the design of a drug-controlled-release matrix, in situ formable scaffold, and the fabrication of precision surface architectures or microdevices using a stereolithographic technique. These will be reported soon.

Acknowledgment. This study was financially supported in part by a Grant-Aid for Scientific Research (Grants A2-12358017 and B2-12470277) from the Ministry of Education, Culture. Sports, Science, and Technology of Japan.

References and Notes

(1) Vert, M. *Angew Makromol. Chem.* **1989**, *166*, 155.
(2) Langer, R.; Vacanti, J. P. *Science* **1993**, *260*, 920.
(3) Okada, H.; Yamamoto, M.; Heya, T.; Inoue, Y.; Kamei, S.; Ogawa, Y.; Toguchi, H. *J. Controlled Release* **1994**, *28*, 121.
(4) Piskin, E. *J. Biomater. Sci. Polym. Ed.* **1994**, *6*, 775.
(5) Chiellini, E.; Solaro R. *Macromol. Symp.* **1995**, *98*, 803.
(6) Mooney, D. J.; Mazzoni, C. L.; Breuer, C.; McNamara, K.; Hern, D.; Vacanti, J. P.; Langer, R. *Biomaterials* **1996**, *17*, 115.
(7) Hubbell, J. A. *Solid State Mater. Sci.* **1998**, *3*, 246.
(8) Hubbell, J. A. U.S. Patent 6,306, 922, October, 2001.
(9) Mizutani, M.; Matsuda, T. *J. Biomed. Mater. Res.* **2002**, *62*, 395.
(10) Cooke, M. N.; Fisher, J. P.; Dean, D.; Rimnac, C.; Mikos, A. G. *J. Biomed. Mater. Res., Part B: Appl. Biomater.* **2002**, *64B*, 65.
(11) Zhu, K. J.; Hendren, R. W.; Jensen, K.; Pitt, C. G. *Macromolecules* **1991**, *24*, 1736.
(12) Albertsson, A.-C.; Sjöling, M. *J. Polym. Sci., Pure Appl. Chem.* **1992**, *A29*, 43.
(13) Albertsson, A.-C.; Eklund, M. J. *Appl. Polym. Sci.* **1995**, *57*, 1, 87.
(14) Matsuda, T.; Mizutani, M. *Macromolecules* **2000**, *33*, 791.
(15) Matsuda, T.; Mizutani, M.; Arnold, S. C. *Macromolecules* **2000**, *33*, 795.
(16) Mizutani, M.; Matsuda, T. *Biomacromolecules* **2002**, *3*, 249.
(17) Matsuda, T.; Mizutani, M. *J. Biomed. Mater. Res.* **2002**, *61*, 53.
(18) Matsuda, T.; Mizutani, M.; Arnold, S. C. *Biomacromolecules* **2002**, *3*, 668.
(19) Matsuda, T.; Mizutani, M. *J. Biomed. Mater. Res.* **2002**, *62*, 387.
(20) Weisenhorn, A. L.; Khorsandi, M.; Kasas, S.; Gotzos, V.; Butt, H.-J. *Nanotechnology* **1993**, *4*, 106.
(21) Sneddon, I. N. *Int. J. Eng. Sci.* **1965**, *3*, 47.
(22) Benoît, H.; Grubisic, Z.; Rempp, P.; Decker, D.; Zilliox, J. G. *J. Chim. Phys.* **1966**, *63*, 1507.

BM034231K

TISSUE ENGINEERING
Volume 10, Number 3/4, 2004

Photocured, Styrenated Gelatin-Based Microspheres for *de Novo* Adipogenesis through Corelease of Basic Fibroblast Growth Factor, Insulin, and Insulin-Like Growth Factor I

TEIICHI MASUDA, M.D.,[1,2] MASUTAKA FURUE, M.D., Ph.D.,[2] and TAKEHISA MATSUDA, Ph.D.[1]

ABSTRACT

***De novo* adipose tissue formation appears to proceed via two different biological events: neovascularization and spontaneous accumulation of preadipocytes and subsequent differentiation to mature adipocytes. In this article, we perform accelerated *de novo* adipose tissue engineering using photocured, styrenated, gelatin-based microspheres (SGMs) with different drug release rates of immobilized angiogenic and adipogenic factors. The concept of this system is to induce neovascularization and migration of endogenous preadipocytes by the rapid delivery of the angiogenic factor basic fibroblast growth factor (bFGF), followed by the proliferation and differentiation of preadipocytes into adipocytes by the prolonged delivery of the adipogenic factors, insulin and insulin-like growth factor I (IGF-I). Bioactive substance-immobilized SGMs with different drug release rates were prepared with different gelatin concentrations. An *in vitro* study showed the prolonged release of an immobilized model protein and the dependence of drug release rate on gelatin concentration. After the subcutaneous injections of SGMs immobilized with these bioactive substances in different combinations, the formation of masses or clusters of adipocytes was observed in rats. Triglyceride content in the injection site for the group that received bFGF-, insulin-, and IGF-I-immobilized SGMs was significantly higher than that for the group that received insulin- and IGF-I-immobilized SGMs 4 weeks after the injection of microspheres. These results suggest that the system developed here is effective for the *de novo* formation of adipose tissue as it enables the induction of the two-step biological reaction by single injection.**

INTRODUCTION

SOFT TISSUE AUGMENTATION is still an ongoing challenge in the field of plastic and reconstructive surgery. The use of adipose tissue equivalents is required for the treatment of soft tissue defects such as congenital malformations (e.g., hemifacial microsomia and Poland's syndrome) and posttraumatic or postoperative wounds. The available clinical approaches to overcoming these issues include local–regional or free microvascular flaps, dermal fat graft, collagen injection, the use of synthetic materials, and autologous fat transplantation. Each of these methods, however, is associated with certain drawbacks such as operative risk to some degree, donor site morbidity, resorption of implanted grafts, and foreign body reaction to the implanted synthetic materials.[1–4]

The tissue-engineering approach to forming adipose

[1]Department of Biomedical Engineering, Graduate School of Medicine, Kyushu University, Fukuoka, Japan.
[2]Department of Dermatology, Graduate School of Medicine, Kyushu University, Fukuoka, Japan.

tissue can be realized via two methods: one method is to transplant preadipocytes with or without a scaffold into the site in which soft tissue repair is required, followed by the spontaneous differentiation of preadipocytes or adipocyte progenitor cells to mature adipocytes,[5-10] and the other method is *de novo* adipogenesis, which proceeds via a two-step biological process. First, the enhanced migration of preadipocytes is accompanied by induced local neovascularization, followed by the subsequent adipogenic differentiation of preadipocytes to mature adipocytes.[11-14] Regardless of the type of approach, neovascularization appears to be essentially required to avoid necrosis and possibly to secrete unknown differentiation factors. These two different biological events of angiogenesis and adipogenesis have been proven to be promoted by the addition of basic fibroblast growth factor (bFGF) for the former process and insulin and insulin-like growth factor I (IGF-I) for the latter process.[11-16]

For example, *de novo* adipogenesis was realized by injecting a mixed solution of an extract of a basement membrane (Matrigel) and bFGF[11] or gelatin microspheres immobilized with bFGF,[12,13] or by injecting poly(lactic-co-glycolic-acid)-polyethylene glycol (PLGA/PEG) microspheres coimmobilized with insulin and IGF-I into the subcutaneous lesion.[14] However, an attempt at long-term simultaneous delivery of both angiogenic and adipogenic factors to generate adipose tissues has not yet been reported.

Our approach toward *de novo* adipose tissue formation aims at the construction of a long-term simultaneous delivery system for angiogenic (bFGF) and adipogenic (insulin and IGF-I) factors, both of which are separately immobilized in photocured, styrenated gelatin microspheres (SGMs). Our previous study showed that a photocured SG matrix can serve as a drug delivery system with the following features: (1) the desired amount of drug in a photocured matrix can be easily loaded and (2) the drug release rate can be controlled.[17]

Our strategy by which *de novo* adipose tissue formation is accelerated involves coinjection of three different types of photocured SGMs, each of which is immobilized with protein drugs of different biological activities. Because an ideal scenario of *de novo* adipogenesis involves a sequential or simultaneous process of capillary formation and accumulation and differentiation of preadipocytes to adipocytes, co-use of SGMs with the fast release characteristic of bFGF and SGMs and the relatively slow release characteristic of both insulin and IGF-1 may be beneficial. In this study, the preparation of SGMs, and their *in vitro* drug release characteristics, are described and the adipogenic effects on implantation of these microspheres into subcutaneous lesions of rats are examined.

MATERIALS AND METHODS

Materials

Gelatin (from bovine bone; MW, 9.5×10^4 g/mol) was purchased from Wako Pure Chemical Industries (Osaka, Japan). Water-soluble carboxylated camphorquinone (CQ), (1S)-7,7-dimethyl-2,3-dioxobicyclo[2.2.1]hepatane-1-carboxylic acid, was prepared according to the method described previously.[18] Rhodamine–lactalbumin, fluorescein isothiocyanate (FITC)–insulin, and 3,3-diaminobenzidine were purchased from Sigma (St. Louis, MO). Recombinant human basic fibroblast growth factor (bFGF) was purchased from R&D Systems (Minneapolis, MN). Recombinant human IGF-I was purchased from Genzyme (Cambridge, MA). Anti-human von Willebrand factor antibody and peroxidase-conjugated anti-rabbit IgG antibody were purchased from DakoCytomation (Carpinteria, CA). Cryostat specimen matrix (Tissue-Tek O.C.T. compound) was purchased from Sakura Finetek Japan (Tokyo). All other reagents were purchased from Wako Pure Chemical Industries.

Preparation of styrenated gelatin microspheres

The synthesis of photocurable, styrenated gelatins (styrene content, approximately 27.6 per gelatin molecule) and preparation of aqueous styrenated gelatin solutions were carried out according to procedures reported previously.[17] Briefly, styrenated gelatin was synthesized by condensation reaction of gelatin with 4-vinylbenzoic acid. The reaction mixture was dialyzed and then lyophilized, using a freeze-drier. One gram of aqueous styrenated gelatin solution was poured into 20 mL of liquid paraffin with 0.2% Span 85 and stirred at 120–150 rpm under visible light irradiation, using an 80-W halogen lamp (Tokusou Power Lite; Tokuyama, Tokuyama, Japan; wavelength, 400 nm $< \lambda <$ 520 nm; irradiation intensity, 1.3×10^6 lux) for 20 min. After the addition of 20 mL of hexane, the gelatin microspheres formed were collected by filtration through a glass fiber filter (pore size, 0.6 μm). The microspheres were then washed three times with 40-mL aliquots of hexane to remove residual paraffin, and dried for 1 h at room temperature. SGMs were used in further *in vitro* or *in vivo* experiments immediately after preparation.

Morphological analysis of microspheres

SGM morphology was determined by scanning electron microscopy (SEM) (JSM-6301F; UEOL, Tokyo, Japan). Particle size was determined on the basis of randomly selected 500 microspheres from 5 fields of view, using an optical microscope (TE300; Nikon, Tokyo, Japan) fitted with a micrometer scale.

In vitro *drug release*

Two hundred milligrams of aqueous gelatin solution containing 0.1 wt% CQ and 0.2 wt% rhodamine–lactalbumin or FITC–insulin as model drugs, was poured into the bottom of a well of a 48-well dish, and then irradiated with 1.3×10^6 lux of visible light for 3 min to form a gel. Disk-type gels were dispensed into a 12-well dish. Two milliliters of phosphate buffer solution (PBS, pH 7.4) supplemented with penicillin and streptomycin was added to each well and liquid samples were withdrawn from the wells at regular intervals at 37°C. The amount of model drug released from the gel was determined spectrophotometrically at 558 nm for rhodamine–lactalbumin and at 493 nm for FITC–insulin, respectively (DU 530; Beckman Coulter, Fullerton, CA).

In vivo *experiments*

Animal experiments were reviewed by the Committee on the Ethics of Animal Experiments (Faculty of Medicine, Kyushu University, Fukuoka, Japan) and carried out in accordance with the *Guidelines for Animal Experiments* of the Faculty of Medicine, Kyushu University and the law (no. 105) and notification (no. 6) of the Japanese government. Six-week-old male Wistar rats (Kyudou, Saga, Japan) were anesthetized by intraperitoneal injection of pentobarbital (40 mg/kg). Either bFGF, insulin, or IGF-I was premixed with aqueous styrenated gelatin solution, and SGMs were prepared according to the procedure described previously. The gelatin concentrations were 20% for bFGF-immobilized SGMs and 30% for insulin- or IGF-I-immobilized SGMs. One hundred milligrams of bioactive substance-immobilized SGMs was injected subcutaneously into the dorsal area bilaterally. Table 1 details the SGMs used in these experiments, with their various contents of bioactive substances. For group IV, two different SGMs, each immobilized with insulin (2 IU/100 mg of SGM) or IGF-I (2 μg/100 mg of SGM), were prepared separately, and mixed in equal amounts and injected at each site. For group V, three types of SGMs immobilized with either bFGF (3 μg/100 mg of SGM), insulin (3 IU/100 mg of SGM), or IGF-I (3 μg/100 mg of SGM) were prepared and mixed in equal amounts for injection. SGMs without any bioactive substances were used as control. The amount of immobilized insulin was determined approximately from our preliminary animal experiments. That is, a single subcutaneous injection of a quantity 10-fold higher than the total immobilized amount (10 IU of insulin for injected SGMs used for this study) in the backs of rats resulted in death within 1 day of injection, whereas injection of one-tenth the total immobilized amount resulted in no adipose tissue formation. The amount of total immobilized IGF-I was determined from those in previous papers.[14–16] Four rats for each experimental group were used and samples were harvested for further studies.

TABLE 1. EXPERIMENTAL GROUPS[a] AND INGREDIENTS FORMULATION

	Active ingredient (per 100 mg of SG)		
Group no.	*bFGF (μg)*	*Insulin (IU)*	*IGF-I (μg)*
I (0.01)	0.01	—	—
I (0.01)	0.1	—	—
I (1)	1	—	—
I (10)	10	—	—
II	—	1	—
III	—	—	1
IV	—	1	1
V	1	1	1
VI (control)	—	—	—

[a]*Group I:* SGMs immobilized with bFGF at four different concentrations (μg per 100 mg of photocured SG) (group I [0.01 μg], group I [0.1]; group I [1], and group I [10]). *Group II:* SGMs immobilized with 1 IU of insulin per 100 mg of photocured SG. *Group III:* SGMs immobilized with 1 μg of IGF-I per 100 mg of photocured SG. *Group IV:* SGMs immobilized with 1 IU of insulin and 1 μg of IGF-I per 100 mg of photocured SG. *Group V:* SGMs immobilized with 1 μg of bFGF, 1 IU of insulin, and 1 μg of IGF-I per 100 mg of photocured SG. *Group VI:* SGMs immobilized with no ingredient.

Histological studies

Skin paddles with underlying subcutaneous tissue (2×2 cm^2), including the site of injection, were harvested and fixed in 10% formalin. For groups I (0.01) (0.01 μg of bFGF per 100 mg of SGM), I (0.1), I (1), I (10), and VI, the specimens were embedded in paraffin and sectioned, followed by staining with hematoxylin and eosin (H&E) or immunostaining with an antibody to human von Willebrand factor at a dilution of 1:1600 at 4°C for 16 h. After further incubation with the peroxidase-conjugated anti-rabbit IgG antibody, peroxidase activity was visualized with 3,3-diaminobenzidine. The immunostained sections were counterstained with hematoxylin. Twenty different fields were selected from fibrous tissue surrounding residual injected SGMs for determining the number of capillaries (×200 magnification). For groups I (1), II, III, IV, V, and VI, the specimens were divided into two pieces. One-half of each specimen was embedded in paraffin for H&E and von Willebrand factor staining, and the remaining half was embedded in O.C.T. compound, cryosectioned, and stained with Sudan IV.

Lipid analysis

Fibrous tissue (2×2 cm^2), which lies in between the cutaneous muscle of the trunk and the superficial mus-

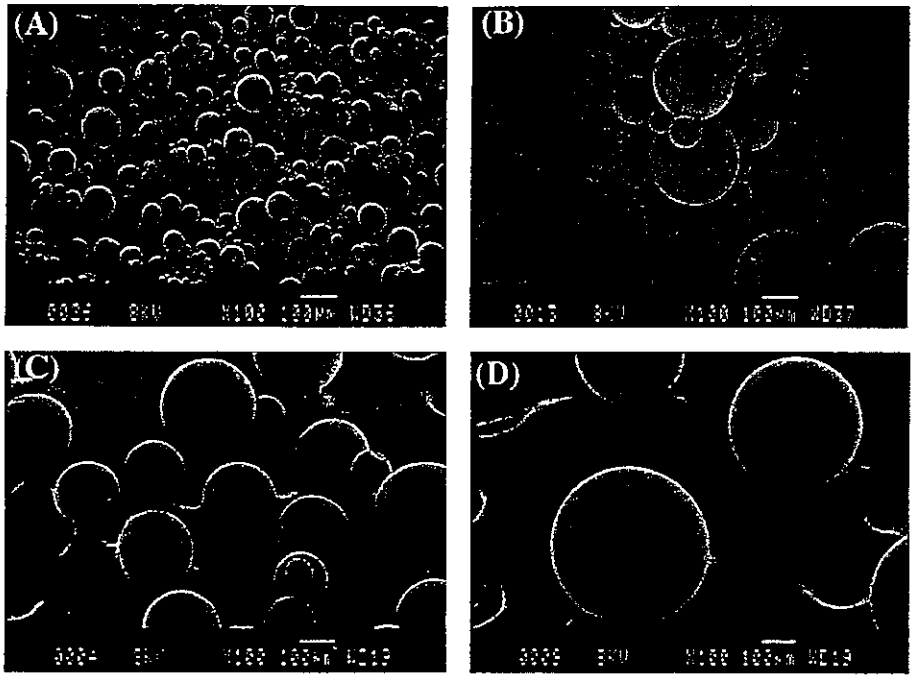

FIG. 1. Scanning electron micrographs of SGMs. SG concentration: (A) 20%, (B) 30%, (C) 40%, (D) 50%.

cles of the back, including the site of SGM injection, was harvested. The specimens were minced and homogenized in distilled water. Total lipid was extracted with chloroform–methanol (2:1, v/v) and centrifuged for 5 min at 1.2×10^4 rpm. The mixed organic solution layer containing triacylglycerol was extracted and placed under vacuum to evaporate the chloroform and methanol. Triacylglycerol content was measured with a triglyceride E-test kit (Wako Pure Chemical Industries) according to the manufacturer's instructions.

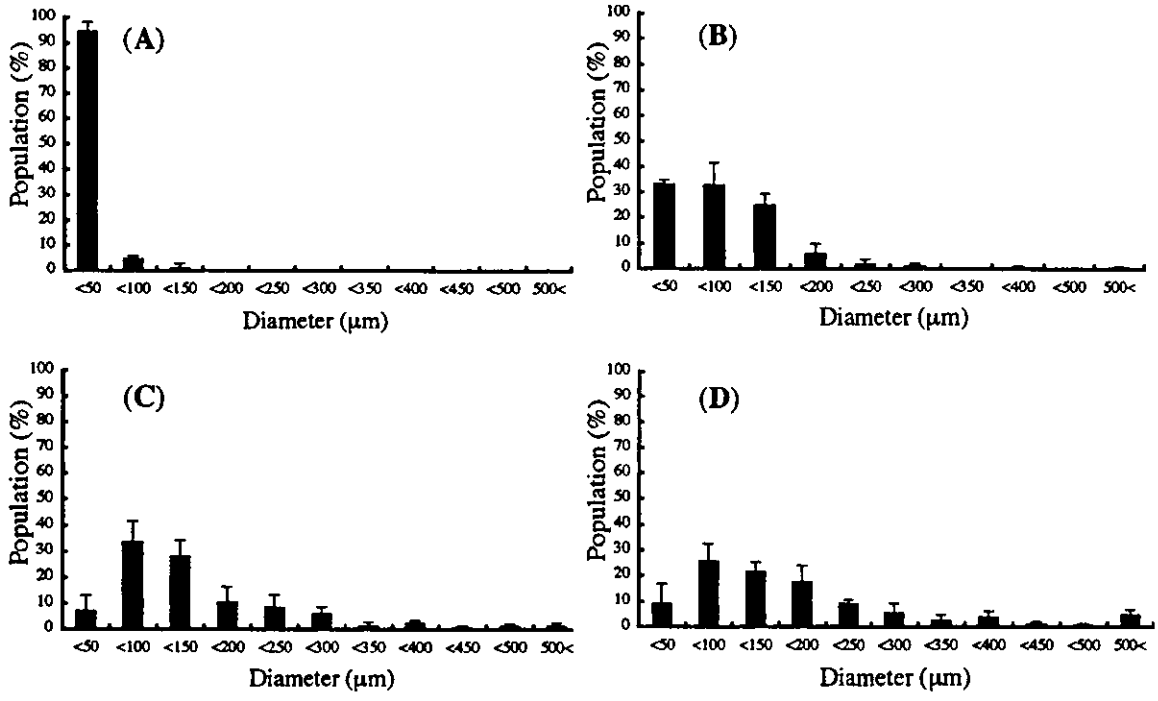

FIG. 2. Particle size distribution of SGMs. SG concentration: (A) 20%, (B) 30%, (C) 40%, (D) 50%.

TABLE 2. MEAN PARTICLE DIAMETER OF SGMs AS FUNCTION OF SG CONCENTRATION

SG concentration (wt %)	*Mean diameter (μm ± SD)*[a]
20	25.4 ± 18.6
30	85.9 ± 69.9
40	145.8 ± 113.4
50	187.1 ± 234.5

Abbreviations: SG, styrenated gelatin; SGMs, styrenated gelatin-based microspheres.

[a]The data were statistically determined on the basis of 500 particles randomly selected from 5 fields of view, using an optical microscope.

Statistical analysis

Experimental results were expressed as means ± standard deviation (SD). The data were subjected to statistical analysis (analysis of variance, ANOVA). Statistical analysis was carried out by ANOVA with a Tukey–Kramer post hoc test; $p < 0.05$ was considered statistically significant. All statistical analyses were performed with StatView 5.0 (Abacus, Berkley, Calif., USA).

RESULTS

Preparation and morphological analysis of photocured gelatin microspheres

Styrenated gelatin (SG)-based microspheres (SGMs) were prepared by dispersing an aqueous solution containing SG and carboxylated camphorquinone as a photocleavable radical generator in liquid paraffin under stirring at room temperature and subsequently subjecting it to visible light irradiation. SEM observations revealed that the SGMs obtained by filtration are fairly round particles with a smooth surface (Fig. 1A–D). Qualitatively, at higher SG concentration, larger microspheres with a broader diameter distribution were obtained. In a quantitative study to determine population size, the obtained histograms show that, at the lowest SG concentration (20%), the size of the majority of microspheres was below 50 μm, and that an increase in SG concentration resulted in a heterogeneous size distribution (Fig. 2A–D). The mean particle diameter of SGMs ranged from approximately 25 to 187 μm, depending on SG concentration (Table 2).

In vitro *drug release*

The SG concentration-dependent release characteristics of model drugs, as shown below, were determined as follows: the photocured SG disks (diameter, 12 mm; thickness, 1.8 mm) were prepared from a premixed solution of SG with a model protein, rhodamine–lactalbumin, the molecular weight of which (1.4×10^4) is almost identical to that of bFGF (1.6×10^4), and FITC–insulin, the molecular weight of which (6.1×10^3) is almost identical to those of insulin (5.7×10^3) and IGF-I (7.6×10^3), at various SG concentrations in the wells of culture dishes. The time course of the release of the model protein into a buffer solution was determined spectrophotometrically. Figure 3A and B shows the time-dependent fractional change in the amount of released rhodamine–lactalbumin and FITC–insulin from SG disks prepared at different SG concentrations, respectively. Irrespective of SG concentration, the release profiles are characterized by an initial burst of protein release during the first day, followed by prolonged release at a lower rate for up to 21 days (length of observation period). The fractional releases of both rhodamine–lactalbumin and FITC–insulin were dependent on SG concentration: the higher the SG concentration, the lower the release rate. Significant differences in release rate were not observed

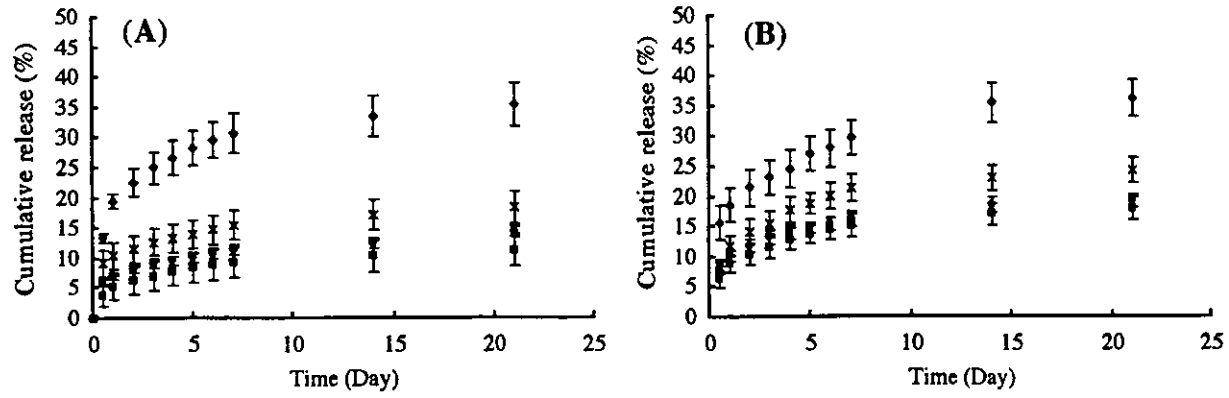

FIG. 3. Fractional release of (A) rhodamine–lactalbumin and (B) FITC–insulin from SG disks ($n = 4$). SG concentration: 20 wt% (◆), 30 wt% (×), 40 wt% (●), and 50 wt% (■). CQ concentration: 0.1 wt% of SG. Visible light irradiation: 3 min at a photointensity of 1.3×10^6 lux. Values are expressed as means ± SD.

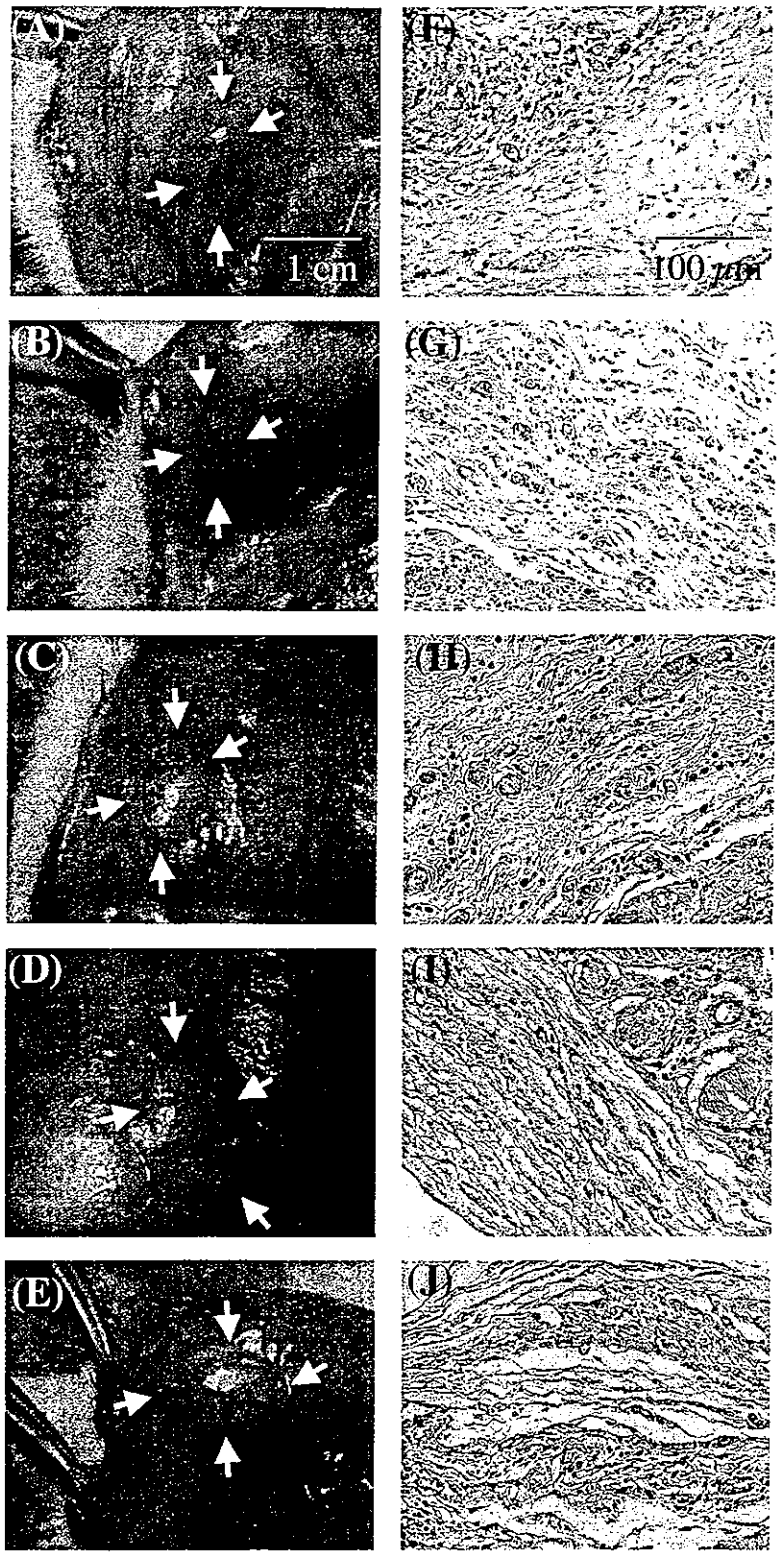

FIG. 4. Tissue appearance (**A–E**, surrounded by arrows) and von Willebrand factor-staining sections (**F–J**) of injection site, 2 weeks after injection of SGMs immobilized with 0.01 [**A** and **F**: group I (0.01)], 0.1 [**B** and **G**: group I (0.1)], 1 [**C** and **H**: group I (1)], 10 [**D** and **I**: group I (10)], and 0 (**E** and **J**: group VI) μg of bFGF.

at a fixed SG concentration, probably because of small difference in the molecular weight of model proteins.

De novo *adipose tissue generation*

Various SGMs immobilized with or without bioactive substances including bFGF, insulin, and IGF-I were prepared at a fixed SG concentration: the SG concentrations used were 20 wt% for bFGF-immobilized SGMs and 30 wt% for insulin- or IGF-I-immobilized SGMs. One hundred milligrams of SGMs was injected into the subcutaneous tissues of Wistar rats. An implantation study was conducted with six different groups as follows. Group I consisted of SGMs immobilized with only bFGF at four different concentrations (μg) per 100 mg of photocured SG, designated Group I (0.01), Group I (0.1), Group I (1), and Group I (10). Group II consisted of SGMs immobilized only with insulin (1 IU per 100 mg of photocured SG), group III consisted of SGMs immobilized only with IGF-I (1 μg per 100 mg of photocured SG), group IV consisted of SGMs immobilized with insulin (1 IU) and IGF-I (1 μg) per 100 mg of photocured SG, and group V consisted of SGMs immobilized with three ingredients (bFGF [1 μg], insulin [1 IU], and IGF-I [1 μg] per 100 mg of photocured SG). Group VI consisted of SGMs immobilized with no bioactive substances.

Effect of bFGF-immobilized microspheres on neovascularization. Figure 4A–E shows macroscopic views of tissues 2 weeks after subcutaneous injection of SGMs with or without bFGF. For Group I, vascularization around the injection site of bFGF-immobilized SGMs became apparent as the amount of bFGF immobilized in SGMs increased. The highest degree of neovascularization was observed for SGMs immobilized with bFGF at a concentration of 1 μg/100 mg of photocured SG, whereas the lowest degree was found for group VI (without bFGF). Figure 4F–J shows results of the histochemical vWF staining of sections of the surrounding tissues in the injection site 2 weeks after the subcutaneous injection of SGMs with or without bFGF. The number of capillaries around the injection site increased as the amount of bFGF immobilized in SGMs increased. The capillary densities of the surrounding tissues 2, 4, and 6 weeks after injection of bFGF-immobilized SGMs, in comparison with those of SGMs without any bioactive substance, are shown in Fig. 5. The highest capillary density was observed for group I (1) 2 weeks after injection, and it was about twice that of the control group (group VI) during the same period; little difference in capillary density was observed 4 and 6 weeks after injection regardless of the group. In comparison with other groups (groups II, III, IV, and V), at 4 weeks postimplantation, there is no significant difference in capillary density between groups, although the mean capillary density of the bioactive substance-immobilized groups, except for the group with the least bFGF, is higher than that of the control (group VI).

Gross observations. Figure 6A–F shows macroscopic views of subcutaneous lesions of groups I (1), II, III, IV, V, and VI, 4 weeks after injection of SGMs immobilized

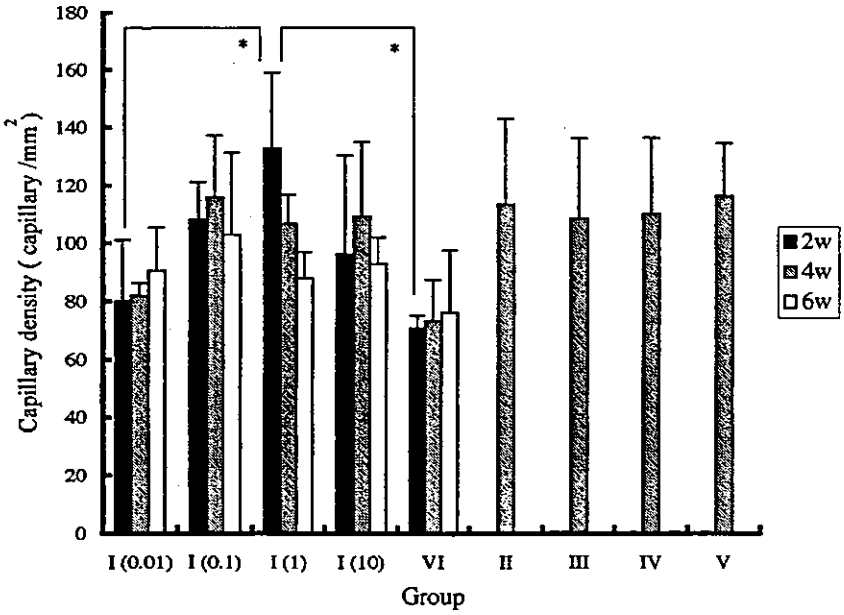

FIG. 5. Capillary density of tissue of the injection site, 2, 4, and 6 weeks after injection of bFGF-immobilized or blank SGMs. Data represent means ± SD. $^*p < 0.05$.

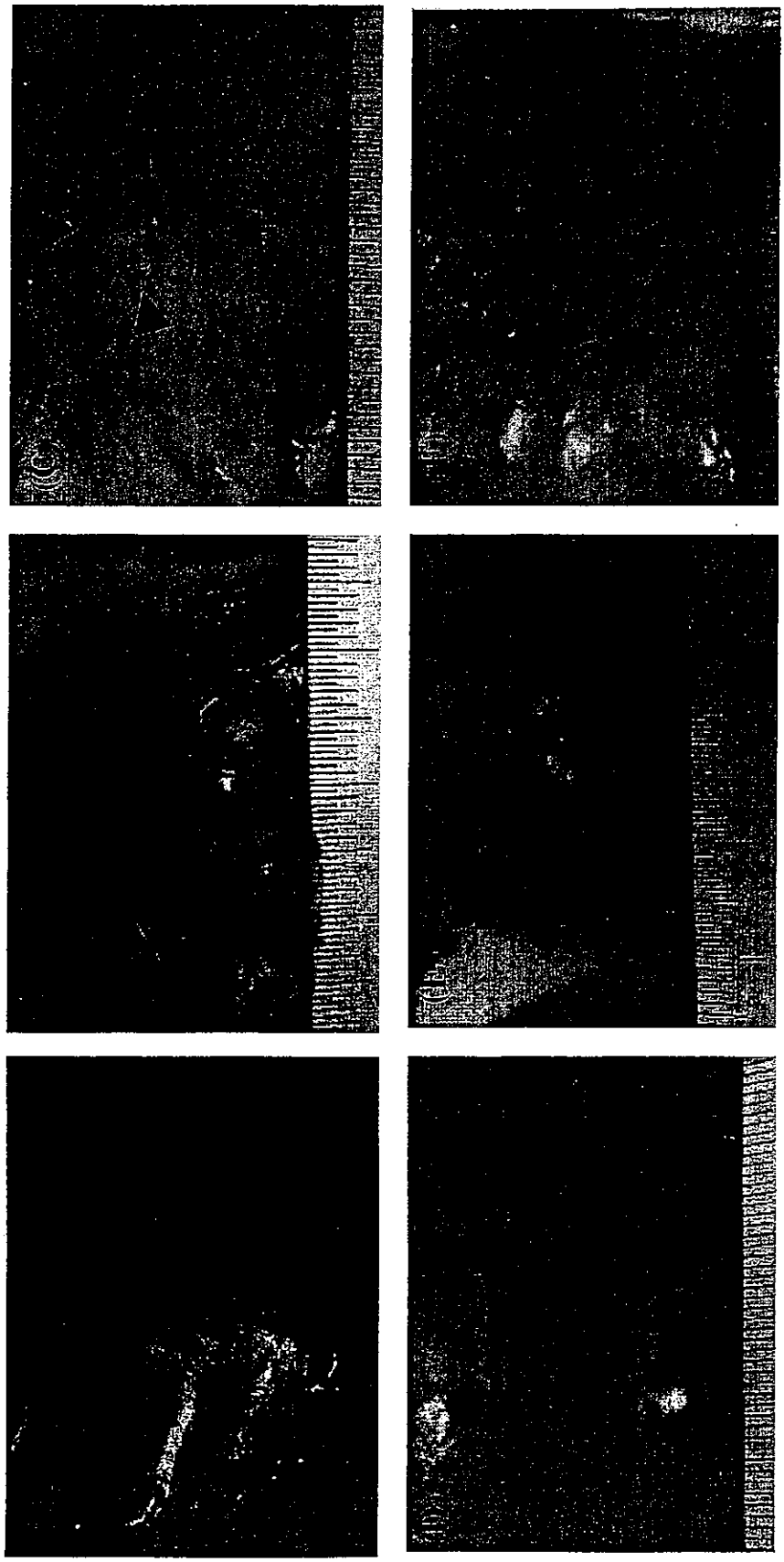

FIG. 6. Tissue appearance of injection site (surrounded by arrows), 4 weeks after injection of SGMs immobilized with various bioactive substances. (A) Group I (1) (SGMs immobilized with 1 μg of bFGF per 100 mg of SG); (B) group II (SGMs immobilized with 1 IU of insulin per 100 mg of SG); (C) group III (SGMs immobilized with 1 μg of IGF-I per 100 mg of SG); (D) group IV (SGMs immobilized with 1 IU of insulin and 1 μg of IGF-I per 100 mg of SG); (E) group V (SGMs immobilized with 1 μg of bFGF, 1 IU of insulin, and 1 μg of IGF-I per 100 mg of SG); (F) group VI (no bioactive substances).

with various bioactive substances. Slightly elevated plaques (approximately 1 × 1 cm^2) were observed at the injection sites of rats in groups I (1), II, III, IV, V, and VI; the most prominent are those of group V (Fig. 6E).

Histology. Figure 7A–L shows the H&E-stained sections of rat subcutaneous lesions of Group I (1), II, III, IV, V, and VI samples 4 weeks after injection of SGMs with or without various bioactive agents. Although partial biodegradation and biosorption occur, residual SGMs remained in all the groups at the injection sites, which were surrounded by tissue composed mainly of collagen fibers and fibroblasts. In groups II–V, masses or clusters of adipocytes were observed between the layers of fibrous tissue. These adipocytes existed in greater number in deeper lesions than in superficial lesions of the residual SGMs. Among these groups, a larger amount of adipose tissue was observed in groups IV and V compared with groups II, III, and VI. In group V, a layer of adipose tissue approximately 1 mm thick was observed adjacent to residual SGMs in deeper lesions. In group VI, however, the injection site was surrounded by a thick layer of connective tissue with few adipocytes interspersed between the layers of fibrous tissue. Sudan IV staining enabled clear visualization of the presence of lipid-containing adipocytes: Sudan IV-positive cells were observed mainly in clusters between the fibrous layers surrounding the residual SGMs, and some cells were also observed among cells that infiltrated residual SGMs (Fig. 8).

Triacylglycerol content. Total lipid at the injection site and surrounding tissue was extracted with chloroform–methanol (2:1, v/v) and triacylglycerol content was determined. In groups IV and V, triacylglycerol content in the surrounding tissues of the injection site were significantly higher than those in groups I (1), III, and VI. Triacylglycerol content in group V was significantly (almost 1.5-fold) higher than that in group IV (Fig. 9).

DISCUSSION

Several studies on the *de novo* formation of adipose tissue by the sustained release of bioactive substances with or without matrixes have been reported. Possible explanations for this adipogenic phenomenon are the migration of endogenous preadipocytes or mesenchymal stem cells into the treated site followed by their pro-

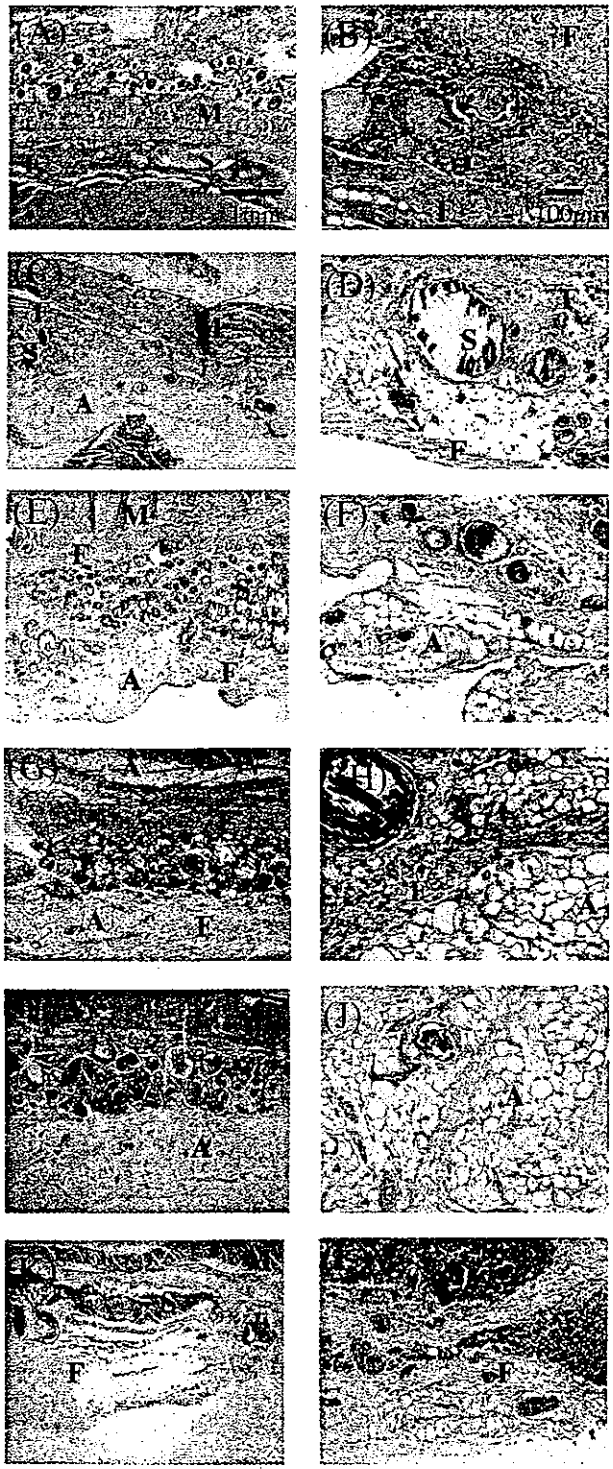

FIG. 7. H&E-stained sections of injection sites, 4 weeks after injection of SGMs immobilized with various bioactive substances. (**A** and **B**) Group I (1) (SGMs immobilized with 1 μg of bFGF per 100 mg of SG); (**C** and **D**) group II (SGMs immobilized with 1 IU of insulin per 100 mg of SG); (**E** and **F**) group III (SGMs immobilized with 1 μg of IGF-I per 100 mg of SG); (**G** and **H**) group IV (SGMs immobilized with 1 IU of insulin and 1 μg of IGF-I per 100 mg of SG); (**I** and **J**) group V (SGMs immobilized with 1 μg of bFGF, 1 IU of insulin, and 1 μg of IGF-I per 100 mg of SG); (**K** and **L**) group VI (no bioactive substances). Original magnifications: (**A, C, E, G,** and **I**) ×20; (**B, D, F, H,** and **J**) ×100. A, Adipose tissue; F, fibrous layer; M, cutaneous muscle of the trunk; S, residual SGMs.

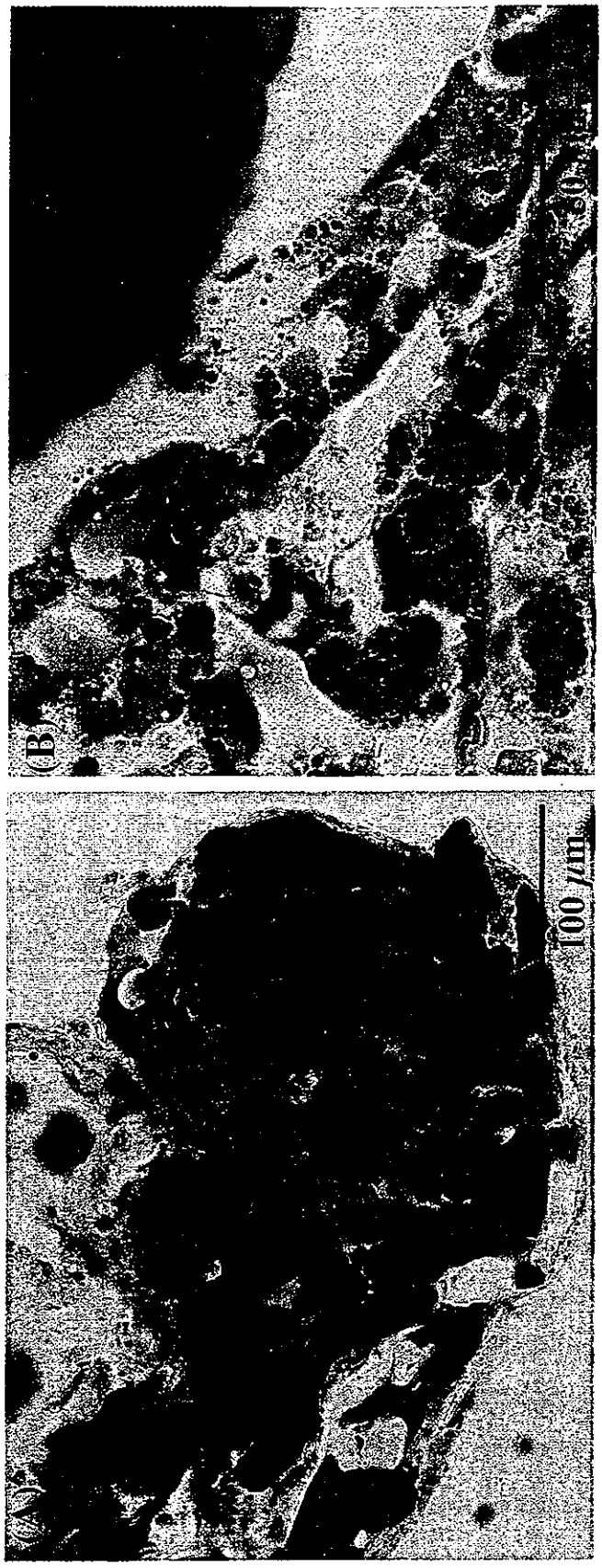

FIG. 8. Representative Sudan IV-stained sections of lipid-containing adipocytes in group V. (A) Adipocytes were observed mainly in clusters between the fibrous layers surrounding the injection site of bioactive substance-immobilized SGMs. (B). Some Sudan IV-positive cells were also observed among cells that infiltrated around residual SGMs.

liferation and differentiation to mature adipocytes.[11–14] Various hormones, cytokines, and growth factors modulate adipocyte differentiation. Among them, insulin and IGF-I separately stimulate adipocyte proliferation and the adipogenic differentiation of nonadipocyte cells to mature adipocytes.[19,20] Angiogenic factors (e.g., bFGF) play a critical role in neovascularization for blood supply and oxygenation, and for recruitment and proliferation of preadipocytes.[11–13,21] For example, the amount of newly formed adipose tissue increased with an increase in the concentration of bFGF, which was immobilized in Matrigel.[11] On the other hand, there appeared to be an optimal dose of bFGF immobilized in gelatin microspheres for adipose tissue formation.[12]

The major issue in adipose tissue regeneration technology is how to accelerate adipose tissue formation and how to regenerate a large amount of adipose tissue in the site of soft tissue defects. One possible means of accelerating adipose tissue formation is to realize the concerted actions of neovascularization and accumulation of preadipocytes, which are driven by the gradual release of angiogenic factors (e.g., bFGF),[11,12,22,23] which should operate in the early phase of implantation, followed by the differentiation of preadipocytes to mature adipocytes as induced by the sustained release of adipogenic factors[14–16] in the later stage. If these two different biological events synchronously or sequentially occur, adipose tissue formation would be accelerated. On the basis of the above-mentioned working principle, we attempted to devise a local drug delivery system that simultaneously releases these biological substances with different release rates. To this end, microspheres made of photocurable, styrenated gelatin were employed as a drug-immobilizing and -releasing matrix.[17] The study on the release characteristics of rhodamine–lactalbumin and FITC–insulin from gel into PBS revealed that the release rate is dependent on SG concentration, independent of the type of model drugs used within the range of the molecular weight tested (approximately 6×10^3–1.4×10^4) (Fig. 3A and B). The release rate was highest for the gel prepared with the lowest gelatin concentration (20%), which was employed for immobilization of bFGF for the rapid release of an angiogenic factor. Denser SGMs, prepared at 30% gelatin concentration, were employed for immobilization of insulin and IGF-I, aiming at a slower release of adipogenic factors than the former version. These microspheres, which were not mechanically fragile, withstood the mechanical stress applied during injection and implantation.

However, it is of importance to verify and discuss how the *in vitro* releasing profile of a protein can correlate with the *in vivo* releasing profile. We did not conduct any such experiment in this study. It is noteworthy to cite briefly a series of studies by Tabata *et al.*[24,25] They used glutaraldehyde-cross-linked "acidic" gelatin (isoelectric point [IEP], 5.0) as a drug carrier, in which bFGF is sorbed from an aqueous solution. *In vitro* releasing from cross-linked gelatin was inhibited because of ionic interaction between bFGF (IEP, 9.6) and acidic gelatin, except for the burst release within the first day of immersion into buffer solution. However, in animal experiments, radioisotope-labeled bFGF was continuously released with implantation time because of proteolytic biodegradation of gelatin. This indicates that *in vitro* releasing characteristics did not reflect *in vivo* releasing characteristics. This must also have occurred in this experiment. Although the IEP of gelatin used in this study was not determined, the *in vitro* releasing profile in Fig. 3A must be due to the

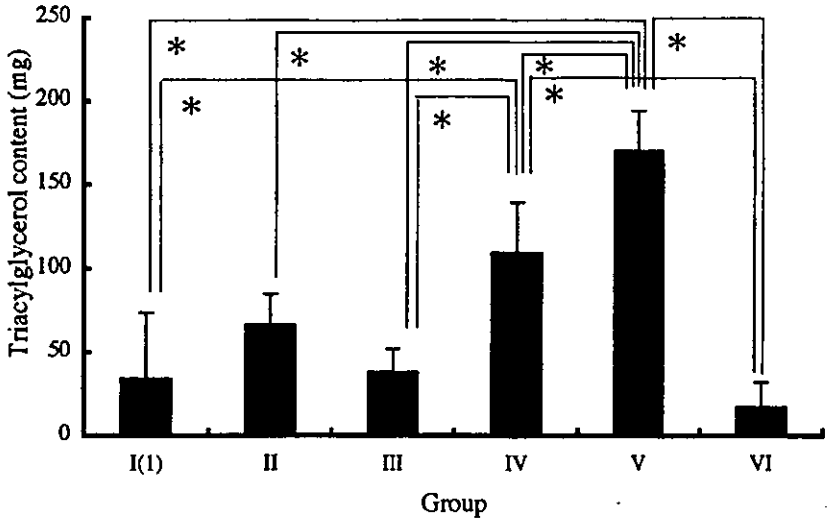

FIG. 9. Total lipid was extracted from SGM injection site tissue and triacylglycerol content was measured as described in Materials and Methods. Data represent means ± SD. $^*p < 0.05$.

combined contribution of size effects of the protein used and some ionic interaction between proteins and gelatin under no proteolytic biodegradation, as mentioned above. Therefore, it is highly anticipated that such a releasing profile does not necessarily correlate with the *in vivo* releasing profile. If biodegradation is a major determinant for release, the time course of released bioactive substances must depend on the degree of photocuring and gelatin concentration, which are principal determinants for biodegradiation as previously reported by us.[17]

A high angiogenesis potential of bFGF-immobilized SGMs was noted (Fig. 4F–J). The capillary densities at the sites treated with bFGF-immobilized SGMs were higher compared with those at the sites treated with SGMs without bFGF (Fig. 5). The capillary density appears to be dependent on bFGF concentration as well as implantation period. At the earlier stage after injection (2 weeks), the highest capillary density was observed at the site treated with group I (1) (1 μg of bFGF immobilized per 100 mg of SG): the capillary density was almost 2-fold higher than that of the site treated with SGMs without bFGF. However, such dependency appears to diminish at a prolonged period after injection (6 weeks). The observed tendency is in good agreement with those previously reported.[26,27] These findings suggest that bFGF released from SGMs induces rapid neovascularization at an early stage after injection.

The study on subcutaneous injection of SGMs immobilized with either an adipogenic factor or combined angiogenic and adipogenic factors clearly showed the possibility of adipose tissue formation (Figs. 7 and 8). Among the groups studied, the largest amount of adipose tissue was observed for the group that received a mixture of three different SGMs, each of which was immobilized with respective bioactive substances (group V). Triacylglycerol content at the site of SGM injection in group V was about 1.5-fold higher than in the group that received a combination of SGMs immobilized with insulin and IGF-I (group IV). This *de novo* adipogenesis is achieved by creating a microenvironment for recruiting endogenous preadipocytes, which subsequently undergo proliferation and differentiation. A single injection of two types of SGMs with two different drug release rates enabled induction of the two-step biological events.

The advantageous features of photocurable gelatin as a drug-immobilized matrix include (1) a controlled degree of cross-linking, which can achieved by the degree of derivatized styrene group in a gelatin molecule, the concentration of styrenated gelatin, and the photocuring time, which is a determinant for the drug-releasing rate as well as the biodegradation rate, and (2) simultaneous photocuring of SG and highly effective immobilization of protein (the amount of protein immobilized can be determined from the formulation during microsphere preparation, due to expected high immobilization efficacy). Water-soluble SG and protein, both of which are not soluble in paraffin, should exist in water phase during microsphere preparation. Therefore, high immobilization efficacy is expected in principle. As for biological activity in immobilized proteins, minor loss of biological activity during photocuring process may not be ruled out. SGMs did not induce substantial damage at cell and tissue levels after the injection of SGMs without any bioactive substances into rat subcutaneous tissue (Fig. 7I and J). Therefore, SGMs can serve as a nontoxic local drug delivery system with easy control of drug immobilization and drug release characteristics.[17]

Although the application of this two-step method for pharmacologically stimulated *de novo* adipose tissue formation is effective, further improvements are required before clinical application of this system. One is to sufficiently increase the amount of newly formed adipose tissue to meet the requirement of soft tissue augmentation and the other is to reduce local fibrosis around injection sites, which occurs with *de novo* adipogenesis. Further studies need to be conducted not only to minimize side effects, but also to maximize the amount of newly formed adipose tissue for soft tissue augmentation. These include optimization of the amount of angiogenic and adipogenic factor, drug release rate, and local inflammation control.

ACKNOWLEDGMENTS

This study was financially supported in part by the Promotion of Fundamental Studies in Health Science of the Organization for Pharmaceutical Safety and Research (OPSR), grant 97-15, and in part by a Grant-in-Aid for Scientific Research (A2-12358017 and B2-12470277) and by a Grant-in-Aid for the Creation of Innovations through Business-Academic-Public Sector Cooperation from the MEXT of Japan. The authors thank Mr. Takaaki Kanemaru (Morphology Core, Graduate School of Medical Sciences, Kyushu University) for SEM observation.

REFERENCES

1. Katz, A.J., Llull, R., Hedrick, M.H., and Futrell, J.W. Emerging approaches to the tissue engineering of fat. Clin. Plast. Surg. **26,** 587, 1999.
2. Billings, E., Jr., and May, J.W., Jr. Historical review and present status of free fat graft autotransplantation in plastic and reconstructive surgery. Plast. Reconstr. Surg. **83,** 368, 1989.
3. Chajchir, A. Fat injection: Long-term follow-up. Aesthetic Plast. Surg. **20,** 291, 1996.
4. Kononas, T.C., Bucky, L.P., Hurley, C., and May, J.W., Jr. The fate of suctioned and surgically removed fat after reimplantation for soft-tissue augmentation: A volumetric and

histologic study in the rabbit. Plast. Reconstr. Surg. **91,** 763, 1993.
5. Green, H., and Kehinde, O. Formation of normally differentiated subcutaneous fat pads by an established preadipose cell line. J. Cell. Physiol. **101,** 169, 1979.
6. Patrick, C.W., Jr., Chauvin, P.B., Hobley, J., and Reece, G.P. Preadipocyte seeded PLGA scaffolds for adipose tissue engineering. Tissue Eng. **5,** 139, 1999.
7. Schoeller, T., Lille, S., Wechselberger, G., Otto, A., Mowlawi, A., and Piza-Katzer, H. Histomorphologic and volumetric analysis of implanted autologous preadipocyte cultures suspended in fibrin glue: A potential new source for tissue augmentation. Aesthetic Plast. Surg. **25, 57,** 2001.
8. von Heimburg, D., Zachariah, S., Heschel, I., Kuhling, H., Schoof, H., Hafemann, B., and Pallua, N. Human preadipocytes seeded on freeze-dried collagen scaffolds investigated in vitro and in vivo. Biomaterials **22,** 429, 2001.
9. Patrick, C.W., Jr., Zheng, B., Johnston, C., and Reece, G.P. Long-term implantation of preadipocyte-seeded PLGA scaffolds. Tissue Eng. **8,** 283, 2002.
10. Halberstadt, C., Austin, C., Rowley, J., Culberson, C., Loebsack, A., Wyatt, S., Coleman, S., Blacksten, L., Burg, K., Mooney, D., and Holder, W., Jr. A hydrogel material for plastic and reconstructive applications injected into the subcutaneous space of a sheep. Tissue Eng. **8,** 309, 2002.
11. Kawaguchi, N., Toriyama, K., Nicodemou-Lena, E., Inou, K., Torii, S., and Kitagawa, Y. *De novo* adipogenesis in mice at the site of injection of basement membrane and basic fibroblast growth factor. Proc. Natl. Acad. Sci. U.S.A. **95,** 1062, 1998.
12. Tabata, Y., Miyao, M., Inamoto, T., Ishii, T., Hirano, Y., Yamaoki, Y., and Ikada, Y. De novo formation of adipose tissue by controlled release of basic fibroblast growth factor. Tissue Eng. **6,** 279, 2000.
13. Kimura, Y., Ozeki, M., Inamoto, T., and Tabata, Y. Time course of de novo adipogenesis in matrigel by gelatin microspheres incorporating basic fibroblast growth factor. Tissue Eng. **8,** 603, 2002.
14. Yuksel, E., Weinfeld, A.B., Cleek, R., Waugh, J.M., Jensen, J., Boutros, S., Shenaq, S.M., and Spira, M. De novo adipose tissue generation through long-term, local delivery of insulin and insulin-like growth factor-1 by PLGA/PEG microspheres in an in vivo rat model: A novel concept and capability. Plast. Reconstr. Surg. **105,** 1721, 2000.
15. Yuksel, E., Weinfeld, A.B., Cleek, R., Jensen, J., Wamsley, S., Waugh, J.M., Spira, M., and Shenaq, S. Augmentation of adipofascial flaps using the long-term local delivery of insulin and insulin-like growth factor-1. Plast. Reconstr. Surg. **106,** 373, 2000.
16. Yuksel, E., Weinfeld, A.B., Cleek, R., Wamsley, S., Jensen, J., Boutros, S., Waugh, J.M., Shenaq, S.M., and Spira, M. Increased free fat-graft survival with the long-term. local delivery of insulin, insulin-like growth factor-I, and basic fibroblast growth factor by PLGA/PEG microspheres. Plast. Reconstr. Surg. **105,** 1712, 2000.
17. Okino, H., Nakayama, Y., Tanaka, M., and Matsuda, T. In situ hydrogelation of photocurable gelatin and drug release. J. Biomed. Mater. Res. **59,** 233, 2002.
18. Matsuda, T., and Magoshi, T. Preparation of vinylated polysaccharides and photofabrication of tubular scaffolds as potential use in tissue engineering. Biomacromolecules **3,** 942, 2002.
19. Caplan, A.I. The mesengenic process. Clin. Plast. Surg. **21,** 429, 1994.
20. Gregoire, F.M., Smas, C.M., and Sul, H.S. Understanding adipocyte differentiation. Physiol. Rev. **78,** 783, 1998.
21. Eppley, B., Sidner, R., Platis, J., and Sadove, M. Bioactivation of free-fat transfers: A potential new approach to improving graft survival. Plast. Reconstr. Surg. **90,** 1022, 1992.
22. Rupnick, M.A., Panigrahy, D., Zhang, C.Y., Dallabrida, S.M., Lowell, B.B., Langer, R., and Folkman, M.J. Adipose tissue mass can be regulated through the vasculature. Proc. Natl. Acad. Sci. U.S.A. **99,** 10730, 2002.
23. Babensee, J.E., McIntire, L.V., and Mikos, A.G. Growth factor delivery for tissue engineering. Pharm. Res. **17,** 497, 2000.
24. Tabata, Y., and Ikada, Y. Protein release from gelatin matrices. Adv. Drug Deliv. Rev. **31,** 287, 1998.
25. Yamamoto, M., Ikada, Y., and Tabata, Y. Controlled release of growth factors based on biodegradation of gelatin hydrogel. J. Biomater. Sci. Polym. Ed. **12,** 77, 2001.
26. Tabata, Y., Hijikata, S., Muniruzzaman, M., and Ikada, Y. Neovascularization effect of biodegradable gelatin microspheres incorporation basic fibroblast growth factor. J. Biomater. Sci. Polymer Ed. **10,** 79, 1999.
27. Tanihara, M., Suzuki, Y., Yamamoto, E., Noguchi, A., and Mizushima, Y. Sustained release of basic fibroblast growth factor and angiogenesis in a novel covalently crosslinked gel of heparin and alginate. J. Biomed. Mater. Res. **56,** 216, 2001.

Address reprint requests to:
Takehisa Matsuda, Ph.D.
Department of Biomedical Engineering
Graduate School of Medicine
Kyushu University
3-1-1 Maidashi, Higashiku
Fukuoka 812-8582, Japan

E-mail: matsuda@med.kyushu-u.ac.jp

Available online at www.sciencedirect.com
SCIENCE DIRECT®
Biomaterials 25 (2004) 5867–5873
Biomaterials
www.elsevier.com/locate/biomaterials

In situ-formed, tissue-adhesive co-gel composed of styrenated gelatin and styrenated antibody: potential use for local anti-cytokine antibody therapy on surgically resected tissues

Tatsuya Manabe[a,b], Hidenobu Okino[a,b], Masao Tanaka[b], Takehisa Matsuda[a,*]

[a] *Divisions of Biomedical Engineering, Graduate School of Medicine, Kyushu University, 3-1-1 Maidashi, Fukuoka City, Fukuoka 812-8582, Japan*
[b] *Division of Surgery and Oncology, Graduate School of Medicine, Kyushu University, 3-1-1 Maidashi, Fukuoka 812-8582, Japan*

Received 24 October 2003; accepted 20 January 2004

Abstract

Styrenated antibody (ST-Ab) and styrenated gelatin (ST-gelatin) were prepared by condensation reaction of antibody or gelatin with 4-vinylbenzoic acid, respectively. The affinity loss of ST-Ab to its antigen was minimal. ST-Ab and ST-gelatin were copolymerized with by visible-light irradiation in the presence of a water-soluble camphorquinone as a photoinitiator to produce a tissue-adhesive, in situ-formed co-gel of ST-gelatin and ST-Ab. The amount of non-reacted ST-Ab released from the co-gel of ST-gelatin and ST-Ab into the medium was minimal. The confocal laser scanning microscopy observation showed that local accumulation of rhodamine-labeled bovine serum albumin (BSA) as a model antigen was noticed in the surface-to-subsurface region of the co-gel of ST-gelatin and anti-BSA ST-Ab, indicating that the gel prevented the permeation of BSA into the gel. In invasion double chamber assay using anti-hepatocyte growth factor (HGF) antibody, the co-gel prevented HGF-dependent invasion of pancreatic cancer cells. The discussion was made for potential application of an in situ-formed tissue-adhesive co-gel of ST-gelatin and ST-Ab, developed in this study, as a cytokine-barrier on a surgically resected tissue where cancer cells might still remain after resection of cancerous tissue.

Keywords: Photoreactive gelatin; Photoreactive antibody; Local antibody therapy

1. Introduction

Various therapeutic approaches toward the cure from cancer, which is one of the most incurable diseases, have been explored and attempted. As for biomaterials-based therapeutic procedures, systemic administration of micelle-type drug and polymer-bound controlled drug delivery system based on biodegradable matrices have been experimentally explored and their therapeutic effectiveness have been proven [1–4]. However, surgical resection is still the first and most effective therapeutic choice when the malignant tissue is localized without distant metastases. As for pancreatic cancer, resection is the only curative modality, but the survival rate of resected patients is still very low [5,6]. The major reason is that pancreatic cancer cells often remain in the retroperitoneal space after surgery, and subsequently induce local recurrence at a high incidence (50–80%) [7]. Therefore, new therapeutic modalities to prevent local recurrence after surgery have been awaited.

Such a malignant behavior is usually accelerated by various cytokines related to inflammations and tissue regenerations after surgery, such as hepatocyte growth factor (HGF), epidermal growth factor (EGF), basic fibroblast growth factor (bFGF), and transforming growth factor-β (TGF-β) [8]. Among them, HGF, which is known to act as multipotent tissue-regenerating and tumor-progressing factor, affects most potently the invasiveness of carcinoma cells [9–17]. HGF is produced and accumulated in the intraperitoneal space after abdominal operation, resulting in an activation of the malignant potentials of remnant cancer cells (Fig. 1A) [17–21].

Recently, monoclonal antibody-based molecular targeting therapy aimed at cytokine deactivation has been developed in cancer treatment [22]. For example, an

*Corresponding author. Tel.: +81-92-642-6210; fax: 81-92-642-6212.
E-mail address: matsuda@med.kyushu-u.ac.jp (T. Matsuda).

0142-9612/$ - see front matter © 2004 Elsevier Ltd. All rights reserved.
doi:10.1016/j.biomaterials.2004.01.036

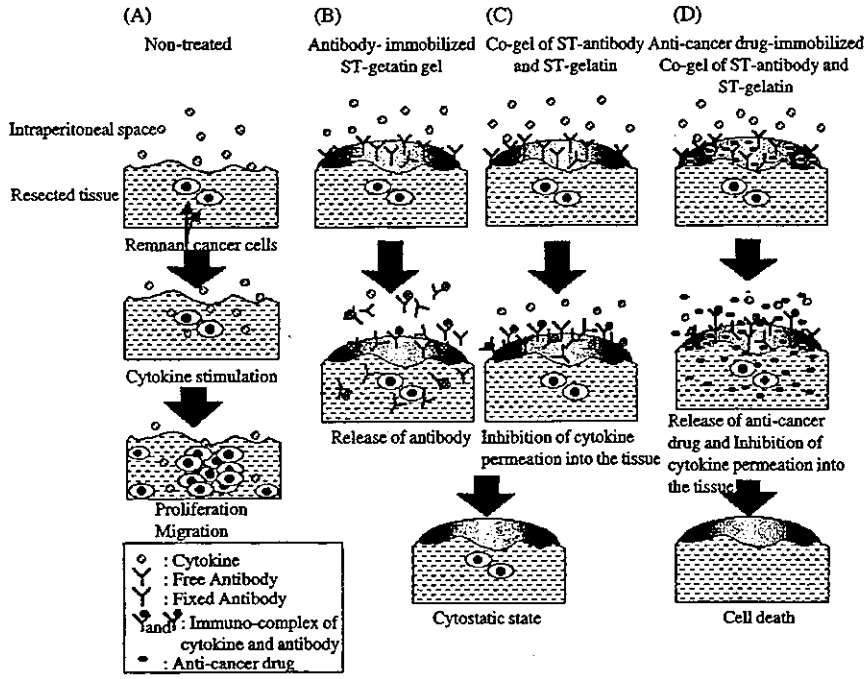

Fig. 1. Schematic of the strategy for local anti-cytokine antibody therapy using in situ photocured gel. (A) Various cytokines produced and accumulated in the intraperitoneal space during wound healing after abdominal surgery and affect remnant cancer cells in surgically resected tissues. (B) Non-treated antibody-immobilized ST-gelatin gel on resected tissues. Antibodies neutralize cytokines in and out of a gel and prevent the effect of cytokines on remnant cancer cells. The antibody-antigen complexes also penetrate into resected tissues. (C) The co-gel of ST-gelatin and anti-cytokine ST-Ab on resected tissues. Antibodies fixed in a gel neutralize cytokines, which permeated into a gel, thereby preventing the permeation and penetration of cytokines into resected tissues. (D) Anti-cancer drug-immobilized co-gel of ST-Ab and ST-gelatin on resected tissue. Cytokine permeation into the tissue was prevented, and anti-cancer drug released from the gel induced cell death.

anti-EGF receptor monoclonal antibody or an anti-vascular endothelial growth factor (VEGF) monoclonal antibody has been systemically administered to reduce the growth of cancerous tissues [23–25]. However, in the early period after surgery, when prompt tissue regeneration accelerated by cytokines is necessary at the resected tissues, particularly the anastomotic site, systemically administered molecular-targeted antibody might induce the inhibition of wound healing. Thus, local antibody delivery must have some advantages because locally delivered antibody could not affect distant site compared with systemic administration.

Previously we have proposed a local delivery system of drugs, proteins or gene-encoding adenoviral vectors using in situ photocured gelatin gel, which is based on styrenated gelatin (ST-gelatin) [26–28]. ST-gelatin is in situ photopolymerized by visible-light irradiation in the presence of a water-soluble camphorquinone as a photoinitiator to produce a gel, which adheres well on surgically resected tissues. In this article, styrenated antibody (ST-Ab) was prepared to copolymerize with ST-gelatin, producing a tissue-adhesive, gelatinous co-gel of ST-gelatin and ST-Ab (Fig. 2A). When the co-gel of ST-gelatin and anti-cytokine ST-Ab is produced on surgically resected tissue where cancer cells might remain, it was anticipated to work well as a cytokine-barrier (Fig. 1C). Herein we present the preparation of ST-Ab and a co-gel of ST-gelatin and ST-Ab, and its in vitro performance, and discuss potential use in clinical settings and new local anti-cytokine therapy using the antibody-bound co-gel.

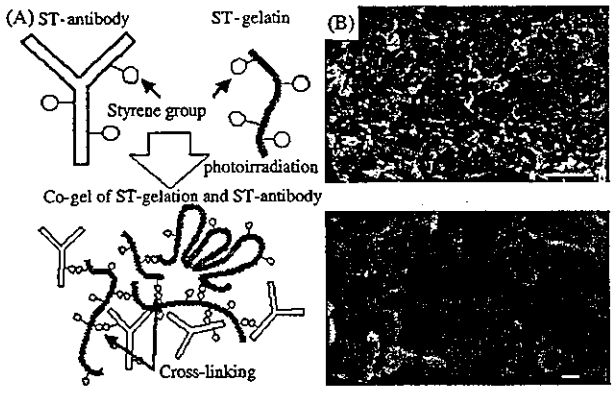

Fig. 2. (A) ST-gelatin (MW 95,000), ST-Ab (MW 150,000), and their polymerization. The average numbers of styrene groups derivatized into gelatin and antibody molecule were approximately 27.3 and 5.1, respectively. Photogelation mechanism by formation of inter- and intramolecular polymerization of ST-gelatin and ST-Ab. (B) SEM observation showed the network mesh and multiple micropores of the surface structure of the co-gel. Bar: 1 μm in upper figure; 100 nm in lower figure.

2. Methods

2.1. Materials

The reagents used and their suppliers were as follows: bovine serum albumin (BSA, MW 6.6×10^4 g/mol) and gelatin (from bovine, MW 9.5×10^4 g/mol) from Wako Pure Chemical Ind., Inc. (Osaka, Japan); 4-vinylbenzoic acid from Tokyo Chemicals Inc., Co., Ltd. (Tokyo, Japan); 1-ethyl-3-(3-dimethylaminopropyl)carbodiimide hydrochloride (WSC) from Dojindo Laboratory (Kumamoto, Japan); rhodamine-conjugated BSA from Sigma-Aldrich Inc. (St. Louis, MO); anti-BSA rabbit IgG antibody from Rockland Inc. (Gilbertsville, PA); phosphate-buffered saline solution (PBS, pH 7.4) from Nissui Pharmaceutical Co. Ltd. (Tokyo, Japan); and anti-human HGF antibody from Techne Co. (Minneapolis, MN). (1*S*)-7,7-Dimethyl-2,3-dioxobicyclo[2.2.1]-heptane-1-carboxylic acid (carboxylated camphorquinone, CQ) was prepared according to the method described previously [26]. The preparation of ST-gelatin was already described in detail in our previous paper [26–29]. The average number of styrene groups derivatized into a gelatin molecule, determined from its absorbance (4-vinylbenzoic acid at 268 nm) as described previously, was 27.3 per molecule.

2.2. Styrenated antibody

The derivatization of a styrene group to IgG antibody molecules was carried out by similar method to ST-gelatin treatment [26–29]. Briefly, an anti-BSA ST-Ab was prepared as follows (for anti-HGF antibody, the reaction feed was scaled down): 4-Vinylbenzoic acid (5.9 mg, 3.98×10^{-5} mol) was dissolved in 15 ml of 0.1 N sodium hydroxide and then neutralized to pH 7.5 with hydrochloric acid. After the addition of WSC (246.7 mg, 1.28×10^{-3} mol), the reaction solution was stirred at 4°C for 30 min and mixed with the anti-BSA antibody (10 mg, 6.7×10^{-8} mol) dissolved in 15 ml of PBS. The reaction mixture was stirred at 4°C for 1 h, dialyzed, and lyophilized to yield a white powder (ST-Ab). The average number of styrene groups derivatized into the antibody molecule, determined from its absorbance, was approximately 5.1 for both anti-BSA and anti-HGF ST-Ab.

The affinity of anti-BSA ST-Ab to its antigen was determined by enzyme-linked immunosorbent assay (ELISA) and compared with that of the non-treated anti-BSA antibody. Using a 96-well microtiter plate (Corning Inc., NY), coated with BSA at various concentrations (50, 100, and 500 ng/50 μl), blocked with 2% sheep serum (Sigma-Aldrich, Inc.) and subsequently washed 3 times with PBS, 60 μl of either non-treated anti-BSA antibody solution (10 μg/ml) or anti-BSA ST-Ab solution (10 μg/ml) was added to the well and the plate was incubated for 1 h at room temperature. After washing five times with PBS, 100 μl of 1:10,000 alkaline phosphatase-conjugated anti-rabbit IgG goat IgG (Sigma-Aldrich, Inc.) was added to the well and the plate was again incubated for 1 h at room temperature. Then, 100 μl of pNPP substrate (4-nitrophenyl phosphate disodium salt solution, Sigma-Aldrich, Inc.) was added and color development, as a quantitative measure of the level of antigen–antibody complex based on coloration, was monitored at 405 nm using a spectrophotometer (Bio-Rad Laboratories, Inc., Hercules, CA).

2.3. Preparation of co-gel of ST-gelatin and ST-Ab and scanning electron microscopic observation

ST-gelatin solution (30 wt%) was used in this study because its viscosity and adhesive strength were optimum [26]. A typical co-gel of ST-gelatin and ST-Ab was prepared as follows. The solution containing 700 μl of PBS, 300 mg of ST-gelatin (30 wt% based on the total gel weight), 2 mg of ST-Ab (0.2 wt% based on the total gel weight), and 0.15 mg of CQ (0.05 wt% based on the ST-gelatin weight) were stirred thoroughly with a high-speed rotating shaker (MX-201, Thinky Co. Ltd., Tokyo, Japan). Then, the solution was photogelled upon visible-light irradiation using an 80-W halogen lamp (Tokuso Power Lite, Tokuyama Co. Ltd., Tokuyama, Japan) (Fig. 2A). Light intensity was 1.3×10^6 lx as measured with a photometer (ANA-F11, Tokyo Kohden Co. Ltd., Tokyo, Japan). The co-gel was fixed in 2% glutaraldehyde (Electron Microscopy Sciences, Morris Road, Washington, PA) for 1 h and then postfixed in 1% osmium tetroxide (Chiyoda Junyaku, Tokyo, Japan) for 1 h, and subsequently dehydrated with a graded series of ethanol, sputter-coated with platinum and evaluated by scanning electron microscopy (SEM) (JEOL, JSM-840A, Tokyo, Japan).

2.4. Release of non-reacted ST-Ab and permeation of antigen

To assess the reaction of copolymerization between ST-gelatin and ST-Ab, the amount of antibody released from the co-gel was examined compared with non-treated antibody-immobilized gel using western blot analysis. Disk-type photocured gels (150 mg; 78.5 mm^2), which were composed of ST-gelatin (30 wt%) in Group 1, ST-gelatin (30 wt%) and non-treated anti-BSA rabbit antibody (0.2 wt%) in Group 2, and ST-gelatin (30 wt%) and anti-BSA rabbit ST-Ab (0.2 wt%) in Group 3, were immersed in 1 ml of PBS for 24 h, and then the supernatants were collected and subjected to western blot analysis. The proteins released from the gels were fractionated by 10% sodium dodecyl sulfate-polyacrylamide gel electrophoresis and transferred to a polyvinylidene difluoride membrane (Millipore,

Bedford, MA). The membrane was incubated with 1: 200 FITC-conjugated anti-rabbit IgG antibody and then photographed using a Molecular Imager FX (Bio-Rad Laboratories Inc.).

To determine the inhibitory effect of the co-gel of ST-gelatin and anti-BSA ST-Ab for permeation of the antigen, three different disk-shaped mixed gels were immersed in 5 ml of 26.4 μg/ml rhodamine-conjugated BSA solution. After 24, 36, and 60 h of incubation at 37°C, the maximum transverse cryostat sections of the gels were prepared with a microslicer (CM 1850, Leica, Nussloch, Germany). The sections were observed and quantitatively determined from the depth profile of fluorescence intensity from the surface using a confocal laser scanning microscopy (CLSM, 595 nm excitation, Bio-Rad Laboratories Inc.).

2.5. Invasion assay

To assess the inhibitory effect of the co-gel as a cytokine-barrier, HGF-dependent invasion of tumor cells was measured with the co-gel of ST-gelatin and anti-HGF ST-Ab using a 24-well Matrigel invasion double chamber (Becton Dickinson, Bedford, MA) (Fig. 6A) [13–17]. Pancreatic cancer cells (SUIT-2) [30], generously donated by Dr. H. Iguchi, were cultured and then suspended in DMEM containing 2% fetal bovine serum (FBS) at 37°C in 5% CO_2. The suspension was added to the inner cup of the Matrigel invasion chamber at a density of 5×10^4 cells/cup. After 6 h of cultivation, the medium was removed, and 10 mg each of the photocured gelatin solutions [Group 1, ST-gelatin (30 wt%) only; Group 2, ST-gelatin (30 wt%) and non-treated anti-HGF antibody (0.2 wt%); or Group 3, ST-gelatin (30 wt%) and anti-HGF ST-Ab (0.2 wt%)] was overlayered on the seeded cells and subsequently photogelled. In Group 0, a gel was not used. Then, 500 μl of DMEM with or without 10 or 50 ng/ml human HGF was added to the inner cup. DMEM (750 μl) containing 2% FBS was added to the outer well and the inner cup was inserted into the outer well. After 24 h of cultivation, the pancreatic cancer cells, that degraded the Matrigel and migrated through 8-μm pores of the membrane at the bottom of the inner cup to the opposite side of the membrane, were counted after hematoxylin and eosin staining. Five microscopic fields (× 200) were randomly selected for cell counting.

3. Results

3.1. Co-gel of ST-gelatin and ST-Ab

The anti-BSA ST-Ab and ST-gelatin were prepared using 4-vinylbenzoic acid according to our previous method [26–29]. As shown in Fig. 3, the degree of the affinity of anti-BSA ST-Ab to BSA, as determined by ELISA, was found to be almost the same as non-ST-Ab. To determine whether the anti-BSA ST-Ab was copolymerized with ST-gelatin, the anti-BSA ST-Ab released from the co-gel into PBS was assayed by western blot analysis using three different disk-type gels [Group 1, only ST-gelatin gel (30 wt%); Group 2, ST-gelatin gel (30 wt%) mixed with non-treated anti-BSA rabbit antibody (0.2 wt%); and Group 3, co-gel of ST-gelatin (30 wt%) and anti-BSA rabbit ST-Ab (0.2 wt%)]. As shown in Fig. 4, the amount of heavy

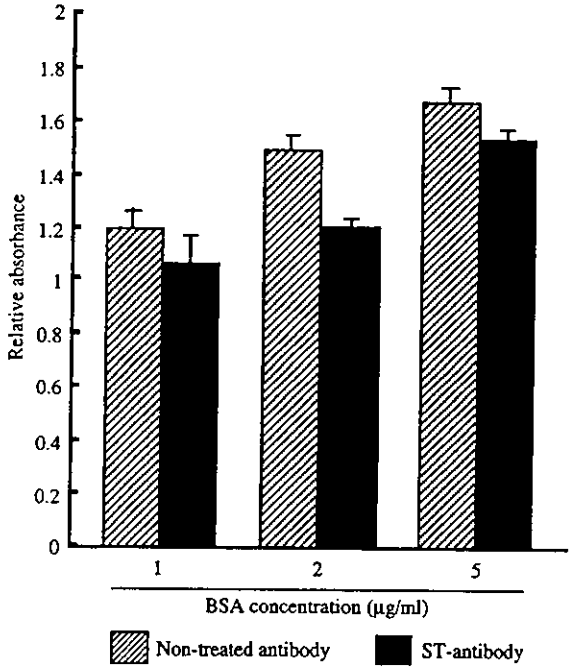

Fig. 3. The affinity of anti-BSA ST-Ab to its antigen was determined by ELISA and compared with that of non-treated anti-BSA antibody ($n = 3$). The affinity of anti-BSA ST-Ab to BSA was observed to be restored.

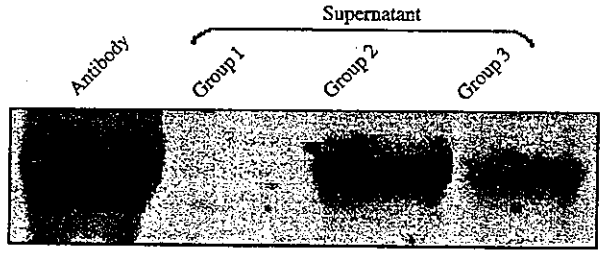

Fig. 4. Amount of ST-Ab released from the co-gel of ST-gelatin and ST-Ab. Disk-type photocured gelatin gels composed of ST-gelatin (Group 1), ST-gelatin and non-treated anti-BSA antibody (Group 2), and ST-gelatin and anti-BSA ST-Ab (Group 3) were immersed in PBS for 24 h, and then the supernatants were collected and subjected to western blot analysis. The amount of heavy chain of the antibody was much larger in Group 2 than in Group 3. This result suggests that a minimal amount of non-reacted ST-Ab is released, indicating that the majority of ST-Ab copolymerizes in a gel.